ELSEVIER

J. Non-Newtonian Fluid Mech. 121 (2004) 127–141

Journal of Non-Newtonian Fluid Mechanics

www.elsevier.com/locate/jnnfm

Modelling the new stress for improved drag reduction predictions of viscoelastic pipe flow

D.O.A. Cruz [a], F.T. Pinho [b,*], P.R. Resende [c]

[a] *Departamento de Engenharia Mecânica, Universidade Federal do Pará-UFPa, Campus Universitário do Guamá, 66075-900 Belém, Pará, Brazil*
[b] *Centro de Estudos de Fenómenos de Transporte, Departamento de Engenharia Mecânica Universidade do Minho, Campus de Azurém, 4800-058 Guimarães, Portugal*
[c] *Centro de Estudos de Fenómenos de Transporte, DEMEGI, Faculdade de Engenharia, Universidade do Porto, Rua Dr. Roberto Frias, 4200-465 Porto, Portugal*

Received 26 January 2004; received in revised form 27 May 2004

Abstract

A model is proposed for the new stress term in the momentum equation of a modified generalised Newtonian fluid that is used to mimic viscoelastic effects of fluids exhibiting drag reduction in turbulent pipe flow. The new stress quantifies the cross-correlation between the fluctuating viscosity and the fluctuating rate of strain and had been neglected in the k-ε low Reynolds number model originally developed by Cruz and Pinho [J. Non-Newt. Fluid Mechanics 114 (2003) 109]. With the inclusion of this new stress, the predictions of turbulent kinetic energy (k^+) in drag reducing pipe flow are significantly improved at the cost of a slight deterioration in the prediction of other quantities for some of the fluids. The value of the coefficient C in the original model of Cruz and Pinho was also modified to correct a mistake and this was shown to improve the predictions for all fluids except for the solution of 0.125% PAA used to calibrate the model. Comparison of predictions with DNS results for a FENE-P model showed large overprediction of drag reduction and emphasize the need for improvements in extensional rheometry.

Keywords: Polymer solution; Drag reduction; Pipe flow; Turbulence model

1. Introduction

The development of turbulence models for drag reducing fluids remains a challenge that is currently motivating a wealth of new research, especially aimed at understanding its relationship with polymer dynamics and fluid rheology. On this front most of the research tends to be based on direct numerical simulation (DNS), such as the works recently reviewed by Pinho [1], to which some recent research must be added.

The most recent DNS research represents the rheology of drag reducing polymer solutions with the FENE-P model [2–4] and there are both advantages and disadvantages in this choice, whereas Zhou and Akhavan [5] show that the FENE-P incurs large errors in predicting extensional flow properties under transient flow conditions (a consistent finding also made by Ptasinski et al. [4]), and recommend multi-mode models or different closures of the basic FENE model, such as the FENE-LS of Lielens et al. [6], Stone and Graham [7] defend the use of FENE-P because of its simplicity and ability to capture relevant features, in spite of its shortcomings. This refers to the overall structure of the stress field, and in particular the large stresses within the buffer layer, and the corresponding fundamental interactions with vortex dynamics that lead to drag reduction, which are the same for the FENE-P as for the full-chain model.

Initial DNS investigations had concentrated on simpler, purely viscous constitutive models to assess different model characteristics. The DNS results of Den Toonder et al. [8,9] had shown only small magnitudes of drag reduction when using scalar viscosities, but a stronger effect associated with anisotropic viscosity and elasticity. In contrast, the turbulent channel flow DNS simulations of FENE-P and Giesekus fluids by Sureshkumar et al. [10] predicted significant drag reduction and showed qualitative agreement with experimental findings, thus emphasizing the strong relationship between drag reduction intensity and the plateau extensional viscosity of polymer solutions, via the extensibility of the polymer

* Corresponding author.
E-mail addresses: doac@ufpa.br (D.O.A. Cruz), fpinho@dem.uminho.pt (F.T. Pinho), resende@fe.up.pt (P.R. Resende).

0377-0257/$ – see front matter © 2004 Elsevier B.V. All rights reserved.
doi:10.1016/j.jnnfm.2004.05.004

Nomenclature

A^+	Van Driest's parameter ($A^+ = 26.5$)
A_ε	turbulence model parameter
B	parameter, $B \equiv \left[\frac{K_v K_e}{A_\varepsilon^{p-1}}\right]^{1-m} 2^{[(n-1)-m(n+1)]/2} \rho^m$
C	turbulence model parameter in f_μ
C_μ	turbulence model parameter
$C_{\varepsilon 1}$	turbulence model parameter
$C_{\varepsilon 2}$	turbulence model parameter
$C_{\varepsilon 4}$	new turbulence model parameter
DR	drag reduction intensity
f	Darcy friction factor
f_F	Fanning friction factor
f_v	damping function of molecular viscosity
f_μ	damping function of eddy viscosity
f_1	damping function in $\tilde{\varepsilon}$ equation
f_2	damping function in $\tilde{\varepsilon}$ equation
H	half-height of a channel
k	turbulent kinetic energy
K_e	viscosity consistency index of Trouton ratio behavior
K_v	shear viscosity consistency index
L	extensibility parameter in FENE-P model
m	parameter defined in Eq. (6)
M	parameter, $m \equiv \frac{n+p-2}{n+p}$
n	shear viscosity power index
$\bar{p}$	mean pressure
p	viscosity power index of Trouton ratio behavior
P_k	turbulence production, defined in Eq. (15)
r	radial coordinate
R	pipe radius
Re_ap	Reynolds number based on apparent viscosity
Re_T	turbulent Reynolds number, defined in Eq. (12)
Re_w	wall Reynolds number
S	invariant of the rate of deformation tensor
s_{ij}	fluctuating rate of deformation tensor
S_{ij}	time-average rate of deformation tensor
t	time
u	local mean velocity
u_i	velocity vector component along coordinate x_i
U	axial mean velocity
u_τ	friction velocity
u_R	characteristic turbulent scaling velocity, defined in Eq. (29)
$-\rho\overline{uv}$	Reynolds shear stress
x	axial coordinate
y	distance measured from the wall
y^+	wall coordinate, defined in Eq. (15)

Greek symbols

β	ratio between solvent and total zero-shear viscosities of FENE-P fluids
$\dot{\gamma}$	invariant measurement of the shear rate (time average value)
$\dot{\gamma}'$	invariant measurement of the shear rate (fluctuating)
δ_{ij}	Kronecker symbol
ε	rate of dissipation of turbulent kinetic energy
$\tilde{\varepsilon}$	modified rate of dissipation of turbulent kinetic energy
$\dot{\varepsilon}$	invariant measurement of the strain rate (time average value)
$\dot{\varepsilon}'$	invariant measurement of the strain rate (fluctuating)
η_e	extensional or elongational viscosity
η_p0	zero-shear polymer viscosity in FENE-P model
η_s	solvent viscosity
η_v	shear (viscometric) viscosity, defined in Eq. (3)
λ	relaxation time of FENE-P model
μ	molecular viscosity
$\bar{\mu}$	true time average molecular viscosity, defined in Eq. (2)
$\bar{\mu}_\mathrm{h}$	time average molecular viscosity for high Reynolds number turbulence, defined in Eq. (4)
ν_T	eddy viscosity
ρ	fluid density
σ_{ij}	stress tensor
σ_k	turbulent Prandtl number for k
σ_ε	turbulent Prandtl number for ε
$\tau_{ij,\mathrm{p}}$	polymer stress (Eqs. (35) and (36))

Subscripts

w	based on wall conditons

Superscripts

+	designates quantities normalised with wall coordinates

chains. So, the DNS simulations have clearly shown that purely viscous constitutive equations cannot predict large drag reductions and that elasticity is required.

However, single-point turbulence closures, which are urgently required for engineering applications, have yet to appear based on these fundamental DNS investigations with viscoelastic constitutive equations. The main difficulty here is that time-averaging of the transport and viscoelastic constitutive equations yields very complex equations, combining new terms with fluctuating stresses, velocities, and their gradients, and their modelling is still unknown. Most likely, as with turbulence models for Newtonian fluids, simplifying assumptions required for closure will be physically incomplete and limited, leading to the adoption of various

damping functions to account for deficiencies. Good examples for Newtonian fluids are the balance equation of ε and the pressure–strain term in the Reynolds stress balance. The higher the complexity of the constitutive equations, the higher the number of new unknowns, and the accuracy of this approach where the apparent advantage of adopting from the outset a better, but more complex, rheological description is offset by many more ad hoc assumptions.

A simpler alternative is at hand based on key widely accepted ideas, relating drag reduction with strain-hardening of the Trouton ratio, as initially put forward by Lumley [11] and confirmed in recent DNS works. Last, but not least, a calculation method should also rely exclusively on fluid rheology and bulk flow characteristics, and not on details of the flows to be determined. Such an approach was put forward by Pinho [1], who developed a framework for single-point turbulence closures based on a modified generalised Newtonian constitutive equation that depended on the second and third invariants of the rate of strain tensor. Although there are several manifestations of viscoelasticity that are not captured by this constitutive equation, the number of terms in the transport equations requiring modelling is significantly reduced and so there are less ad hoc assumptions in the formulation of the turbulence model so that in the end, and at this stage of knowledge and development, this turbulence model can be at least as good as a single-point closure derived from a truly viscoelastic constitutive equation, which we are not aware of. Besides, the current turbulence model, with all its limitations, can also be used in flows of engineering interest, whereas the other available method for viscoelastic fluids (DNS) is simply not feasible with simple computational resources.

The work of Pinho [1], who derived the whole set of equations required for single-point turbulence closures, was pursued by Cruz and Pinho [12], who developed a low Reynolds number k-ε model and compared its predictions with the data of Escudier et al. [13] and Presti [14] which includes both detailed rheological properties and flow characteristics. The advantage of this turbulence model relative to previous single-point closures for viscoelastic fluids, reviewed in Cruz and Pinho [12], is that only parameters related to the shear viscosity and the Trouton ratio need to be used as input data, together with the bulk velocity. However, in their model, Cruz and Pinho [12] neglected a new stress term in the momentum equation and its corresponding effect on the transport of turbulent kinetic energy.

The neglected stress term accounts for the coupling between viscosity fluctuations and rate of strain fluctuations and its role on the transport equation for turbulent kinetic energy is akin to that of any other stress: it can be either a production or a dissipation term. Pinho [1] demonstrated these terms to be smaller than the Reynolds stress terms and negligible for constant viscosity or weakly shear-thinning fluids. However, for strongly shear-thinning fluids, for fluids with a strain-hardening extensional viscosity and in the near vicinity of walls the term may not be so small and helps to improve the predictions especially of the turbulent kinetic energy.

Here, a closed model is proposed to account for this new stress term in the context of low Reynolds number k-ε model of Cruz and Pinho [12] and this is shown to improve predictions for several viscoelastic fluids. As discussed later, the improvement is also due to the correction of a mistake in the model of Cruz and Pinho [12], in the absence of this new stress.

In the next section all the conservation equations, including those of the turbulence model, are presented and the terms requiring modelling are identified. Section 3 proposes a model for the new stress appearing in the momentum and turbulent kinetic energy equations, and the performance of the model is shown in Section 4 via comparisons with experimental data. The paper ends with a summary of the main conclusions.

2. Governing equations

The basic equations to be solved are the Reynolds-averaged mass and momentum equations and those associated with the adopted k-ε turbulence model for fully developed duct flow. The mass equation is not affected by the fluid rheology hence it is not modified. According to Pinho [1], the momentum equation is

$$-\frac{\partial \bar{p}}{\partial x_i} + \frac{\partial(2\bar{\mu}S_{ik} - \rho\overline{u_i u_k} + 2\overline{\mu' s_{ik}})}{\partial x_k} = 0, \tag{1}$$

where p is the pressure, u_i is the i velocity component and S_{ik} is the rate of deformation tensor. Here, and elsewhere, small letters or a prime indicate fluctuations, capital letters or an overbar designate time-average quantities and a hat is used for instantaneous values.

The average molecular viscosity ($\bar{\mu}$) in Eq. (1) is given by the combination in Eq. (2) of a pure viscometric shear viscosity contribution (η_v in Eq. (3)) and the high Reynolds number time-average molecular viscosity contribution ($\bar{\mu}_h$) of Eq. (4):

$$\bar{\mu} = f_v\bar{\mu}_h + (1 - f_v)\eta_v, \tag{2}$$

$$\eta_v = K_v[\dot{\gamma}^2]^{(n-1)/2}, \tag{3}$$

$$\begin{aligned}\bar{\mu}_h = {} & (C_\mu\rho)^{3m(m-1)A_2/(8+3m(m-1)A_2)} \\ & \times 2^{4m(m-1)A_2/(8+3m(m-1)A_2)} k^{6m(m-1)A_2/(8+3m(m-1)A_2)} \\ & \times \varepsilon^{([8-3(m-1)A_2]m)/(8+3m(m-1)A_2)} B^{8/(8+3m(m-1)A_2)},\end{aligned} \tag{4}$$

where K_v and n are the power law parameters, f_v is a damping function and k and ε represent the turbulent kinetic energy and its rate of dissipation, respectively. This viscosity model is based on the following modified constitutive equation [1]:

$$\sigma_{ij} = 2\mu S_{ij}, \tag{5}$$

where the variable viscosity is given by Eq. (6):

$$\mu = \eta_v K_e [\dot{\varepsilon}^2]^{(p-1)/2}. \tag{6}$$

The strain-thickening dependence of μ is quantified by the ratio of the extensional (η_e) to the shear (η_v) viscosities as

$$K_e [\dot{\varepsilon}^2]^{(p-1)/2} = \frac{1}{3}\frac{\eta_e(\dot{\varepsilon})}{\eta_v(\dot{\gamma})}, \tag{7}$$

with $\dot{\gamma} = \sqrt{3}\dot{\varepsilon}$ and K_e and p representing fitting parameters to the Trouton ratio. γ and ε are invariants of the rate of strain tensor. More details of this model can be found in Cruz and Pinho [12].

The Reynolds stresses are expressed by the turbulent viscosity hypothesis

$$-\overline{u_i u_j} = 2\nu_T S_{ij} - \frac{2}{3}k\delta_{ij}, \tag{8}$$

and the turbulent viscosity is specified as a function of k and ε, as for other low Reynolds number models by

$$\nu_T = C_\mu f_\mu \frac{k^2}{\tilde{\varepsilon}}. \tag{9}$$

Hence, the transport equations for k and ε, presented below, must also be solved, and to close the momentum equation it is necessary to determine the new stress $2\overline{\mu' s_{ij}}$. The development of a model for this stress is the main contribution of this work and is addressed in the next section.

The modeled transport equation for k in fully-developed duct flow is

$$0 = \frac{\partial}{\partial x_j}\left[\left(\frac{\bar{\mu}}{\rho} + \frac{\nu_T}{\sigma_k}\right)\frac{\partial k}{\partial x_j}\right] - \frac{2}{\rho}\overline{\mu' s_{ij}} S_{ij} - \overline{u_i u_j} S_{ij} - \varepsilon. \tag{10}$$

This equation differs from that in Cruz and Pinho [12], because the second term on the right-hand-side is now included. The true rate of dissipation ε of k is related to the modified rate of dissipation ε by

$$\varepsilon = \tilde{\varepsilon} + D, \tag{11}$$

where the model of Nagano and Hishida [15] for term D is adopted here, now written for pipe flow

$$D = 2\bar{\nu}\left(\frac{\partial\sqrt{k}}{\partial r}\right)^2. \tag{12}$$

The transport equation for ε is unmodified relative to that of Cruz and Pinho [12] and for fully-developed pipe flow it is given by

$$0 = \frac{1}{r}\frac{\mathrm{d}}{\mathrm{d}r}\left[r\left(\bar{\mu} + \rho\frac{\nu_T}{\sigma_\varepsilon}\right)\frac{\mathrm{d}\tilde{\varepsilon}}{\mathrm{d}r}\right] + \rho f_1 C_{\varepsilon 1}\frac{\tilde{\varepsilon}}{k}P - \rho f_2 C_{\varepsilon 2}\frac{\tilde{\varepsilon}^2}{k} + \rho E + C_{\varepsilon 4}\frac{\nu_T}{\sigma_E \bar{\nu}}\frac{\mathrm{d}\tilde{\varepsilon}}{\mathrm{d}r}\frac{\mathrm{d}\bar{\mu}}{\mathrm{d}r}. \tag{13}$$

Some of the terms and damping functions appearing in this set of equations are

$$E = \bar{\nu}\nu_T(1 - f_\mu)\left(\frac{\partial^2 U}{\partial r^2}\right)^2, \tag{14}$$

$$f_1 = 1.0 \quad \text{and} \quad f_2 = 1 - 0.3\exp(-R_T^2) \quad \text{with } R_T = \frac{k^2}{\bar{\nu}\tilde{\varepsilon}}, \tag{15}$$

$$f_v = f_\mu, \tag{16}$$

and

$$f_\mu = \left\{1 - \left[1 + \left|\frac{1-n}{1+n}\right| y^+\right]^{-|(1+n)/(1-n)|/A^+}\right\} \times \left\{1 - \left[1 + \left|\frac{p-1}{3-p}\right| y^+ C^{(1-p)/(2-p)}\right]^{-|(3-p)/(p-1)|/A^+}\right\}. \tag{17}$$

The wall coordinate is calculated with the friction velocity u_τ and the average molecular shear viscosity at the wall, $\bar{\nu}_w$:

$$y^+ = \frac{u_\tau y}{\bar{\nu}_w}. \tag{18}$$

The remaining turbulence model parameters are listed in Table 1. The Reynolds number used throughout this paper is always based on pipe diameter, bulk flow velocity and wall shear viscosity.

Table 1
Parameters of the low Reynolds k-ε model without the new stress

C_μ	σ_k	σ_ε	$C_{\varepsilon 1}$	$C_{\varepsilon 2}$	$C_{\varepsilon 3}$	A_ε	A_2	C
0.09	1.0	1.3	1.45	1.90	1.0	10	0.45	45

In the original work of Cruz and Pinho [12], a value of $C = 18$ was determined on the basis of comparisons of flow dynamic data, from numerical predictions of their turbulence model, with experimental data of Escudier et al. [13], but by mistake the wrong rheological parameter K_e was used for the solution of 0.125% PAA. Using the correct value of K_e leads to $C = 45$, as shown in Section 4.1.

3. Model for the new stress

Closure of the set of equations of the previous section requires a model for the new stress term $2\overline{\mu' s_{ij}}$ that accounts for the correlation between fluctuations of the viscosity and of the rate of strain tensor. To develop a model for this

stress, estimates are made separately for the viscosity and the rate of strain fluctuations, these are then grouped together and multiplied by a parameter requiring quantification. The model should include dependence on both n and p so that the stress vanishes in the Newtonian limit ($n = 1$, $p = 1$).

By definition [1], the fluctuating viscosity is proportional to

$$\mu' \propto K_v K_e (\dot{\varepsilon}')^{p-1} (\dot{\gamma}')^{n-1}, \tag{19}$$

where the fluctuating invariants γ' and ε' are given by the following expressions

$$\dot{\gamma}' \sim \sqrt{s_{ij}s_{ij}} \quad \text{and} \quad \dot{\varepsilon}' \sim \frac{\sqrt{s_{ij}s_{ij}}}{A_\varepsilon}. \tag{20}$$

A_ε is an empirical parameter, listed in Table 1, used to quantify the relation between shear rates and strain rates within the flow [12].

Calling $S \equiv \sqrt{s_{ij}s_{ij}}$ to denote an invariant quantity, and back-substituting

$$\mu' \propto \frac{K_v K_e}{A_\varepsilon^{p-1}} S^{p+n-2}, \tag{21}$$

and consequently

$$\mu' s_{ij} \propto \frac{K_v K_e}{A_\varepsilon^{p-1}} S^{p+n-2} s_{ij}. \tag{22}$$

Now, estimates must be made for S and s_{ij} as functions of known quantities in order to arrive at a closed set of equations. The estimates are made for S and s_{ij} in the context of a boundary layer and here two assumptions are invoked: (1) that we are in the equilibrium region, where production of turbulence balances its rate of dissipation and (2) that the new stress does not interfere significantly with this equilibrium.

Since, within a boundary layer, $S \sim \partial u'/\partial y$, then

$$P_k = -\rho\overline{uv}\frac{\mathrm{d}U}{\mathrm{d}y} \approx \rho\varepsilon = 2\overline{\hat{\mu}s_{ij}^2} \sim 2\bar{\mu}S^2. \tag{23}$$

Invoking the turbulent viscosity hypothesis for the Reynolds shear stress (Eqs. (8) and (9))

$$\rho C_\mu f_\mu \frac{k^2}{\tilde{\varepsilon}} \left(\frac{\mathrm{d}U}{\mathrm{d}y}\right)^2 \sim 2\bar{\mu}S^2, \tag{24}$$

from which S is estimated to be

$$S = \sqrt{\frac{\rho C_\mu f_\mu (k^2/\tilde{\varepsilon})(\partial U/\partial y)^2}{2\bar{\mu}}}, \tag{25a}$$

or, in more general terms

$$S = \sqrt{\frac{\rho C_\mu f_\mu (k^2/\tilde{\varepsilon}) S_{ij}S_{ij}}{2\bar{\mu}}}. \tag{25b}$$

Within the boundary layer $s_{ij} \approx \partial u_i/\partial x_j \sim \partial u/\partial y$ and $u_i \sim \sqrt{\overline{u_i u_j}}$. Given the model assumed for the Reynolds shear stress (Eq. (8)), the estimate of the velocity fluctuation is

$$u_i \sim \sqrt{C_\mu f_\mu \frac{k^2}{\tilde{\varepsilon}}} \sqrt{\frac{\partial U}{\partial y}}, \tag{26}$$

and the estimate of s_{ij} is

$$s_{ij} \sim \frac{\partial u_i}{\partial x_j} \sim \frac{u_i}{L_c}, \tag{27}$$

L_c is an estimate of spatial scales of turbulence that take into account high Reynolds number flow away from the wall and the damping effect of the approaching wall. Far from the wall

$$L_c = \frac{k^{3/2}}{\varepsilon}, \tag{28a}$$

whereas close to the wall L should be

$$L_c = \frac{u_\tau^3}{\varepsilon}. \tag{28b}$$

To match smoothly these two behaviours, the following general expression is used:

$$\frac{1}{L_c} = \frac{\varepsilon}{u_R^3}, \tag{29a}$$

introducing the velocity scale u_R that matches both limiting behaviours according to

$$u_R^2 = \frac{k}{|\exp(-(k/u_\tau^2)^\alpha) - 1|^{1-\alpha}} \quad \text{with } \alpha = 4. \tag{29b}$$

Therefore, the final expression for the new stress term is

$$2\overline{\mu' s_{ij}} = \tilde{C}\frac{K_v K_e}{A_\varepsilon^{p-1}} \left[\frac{\rho C_\mu f_\mu k^2}{2\bar{\mu}\tilde{\varepsilon}} S_{ij}S_{ij}\right]^{(p+n-2)/2} \times \sqrt{C_\mu f_\mu \frac{k^2}{\tilde{\varepsilon}}} \times \frac{1}{L_c} \times \frac{S_{ij}}{\sqrt[4]{S_{ij}S_{ij}}} \tag{30a}$$

with $1/L_c$ given by Eq. (29). For a fully developed shearing flow, Eq. (30a) is written as

$$2\overline{\mu' s_{xy}} = \tilde{C}\frac{K_v K_e}{A_\varepsilon^{p-1}} \left[\frac{\rho C_\mu f_\mu k^2}{2\bar{\mu}\tilde{\varepsilon}} \left(\frac{\partial U}{\partial y}\right)^2\right]^{(p+n-2)/2} \times \sqrt{C_\mu f_\mu \frac{k^2}{\tilde{\varepsilon}}} \times \frac{1}{L_c} \times \frac{\partial U/\partial y}{\sqrt{|\partial U/\partial y|}}. \tag{30b}$$

The new stress must vanish in the Newtonian limit because there are no viscosity fluctuations, and to arrive at an adequate expression for $\tilde{C}$ the following argument was developed. By definition, the fluctuating viscosity is

$$\mu' = C_1[\hat{S}_{ij}^2]^{(n+p-2)/2} - C_1\overline{[\hat{S}_{ij}^2]^{(n+p-2)/2}}, \tag{31}$$

where C_1 is a parameter [1] for the exact equation, the hat designates instantaneous values and the overbar

time-average values. Assuming $(\overline{\hat{S}_{ij}^2})^a \approx (\overline{s_{ij}^2})^a$ on the basis of high Reynolds number turbulence [16], then

$$\mu' = C_1[(S_{ij}+s_{ij})^2]^{(n+p-2)/2} - C_1[\overline{s_{ij}^2}]^{(n+p-2)/2} \rightarrow \mu' = C_1[\overline{s_{ij}^2}]^{(n+p-2)/2}\left\{\left[\frac{(S_{ij}+s_{ij})^2}{\overline{s_{ij}^2}}\right]^{(n+p-2)/2} - 1\right\}. \quad (32)$$

The term within the curly braces must vanish in the Newtonian limit ($n = p = 1$):

$$\left[\frac{(S_{ij}+s_{ij})^2}{\overline{s_{ij}^2}}\right]^{(n+p-2)/2} - 1 = \left[\left(\frac{S_{ij}}{\sqrt{\overline{s_{ij}^2}}} + \frac{s_{ij}}{\sqrt{\overline{s_{ij}^2}}}\right)^2\right]^{(n+p-2)/2} - 1 \sim [(C_0+1)^2]^{(n+p-2)/2} - 1, \quad (33)$$

hence we arrive at the form of C that contains the parameter to be quantified, C_0:

$$\tilde{C} = (1+C_0)^{p+n-2} - 1. \quad (34)$$

The model for the new stress in Eq. (30a) can be expressed as the product of the time-average rate of deformation tensor (S_{ij}) by a coefficient akin to a second turbulent viscosity that also depends on the mean and turbulent flow fields. This has advantages in terms of the numerical solution of the momentum equation because the new stress is easily introduced into the code via an extra turbulent viscosity.

4. Results and discussion

To assess the performance of the new turbulence model we follow the same philosophy as Cruz and Pinho [12]: using the experimental data of Escudier et al. [13] and Presti [14] for the aqueous solution of 0.125% PAA, the effect of the new stress is investigated first and the model is then optimized through quantification of C_0 and C. Then, simulations with the new model are carried out for the other fluids in their works, and the results compared with the corresponding experimental data. However, prior to the investigation of the effect of the new stress, a correction to the original model of Cruz and Pinho [12] is made in the next section.

The numerical simulations were carried out with the same finite-volume code used in Ref. [12], a modified version of the code of Younis [17] for boundary layer flows. Non-uniform meshes of 199 cells across the pipe were used, having at least 12 computational cells within each of the viscous sublayers ($y^+ < 5$). This computational grid gives mesh-independent results for Newtonian and non-Newtonian fluids within 0.1%.

Table 2
Parameters of viscosity law of Eqs. (3)–(7) used to fit the viscosity data in Ref. [13]

Fluid	K_v (Pas^n)	n	K_e	p
0.25% CMC	0.2639	0.6174	2.0760	1.2678
0.09% CMC/0.09% XG	0.15178	0.5783	2.1833	1.1638
0.2% XG	0.2701	0.4409	3.8519	1.2592
0.125% PAA	0.2491	0.425	8.25[a]	1.4796

[a] Correct value.

4.1. Behaviour of the model without the new stress

The rheological parameters for the 0.125% PAA solution are $K_v = 0.2491\,\text{Pas}^{0.425}$, $n = 0.425$, $K_e = 8.25$ and $p = 1.4796$ as seen in Table 2 that contains information for the other fluids tested. By mistake, in Cruz and Pinho [12] a value of $K_e = 1.9394$ was used for the 0125% PAA solution, instead of the correct value of 8.25, thus underpredicting the extensional viscosity of this fluid by a factor of about 4, as can be seen in Fig. 1(a). Note that all other rheological parameters are correct, for the 0.125% PAA solution (see Fig. 1(b) for the shear viscosity) and the other fluids.

As a consequence, and since the solution of 0.125% PAA is used to calibrate the turbulence model, the correct value of C (appearing in the damping function f_μ) should be 45 instead of 18. The effect of this difference can be assessed in Figs. 2–4, which compare the performance of the various turbulence models in this work with the corresponding experimental data. Clearly, the use of $C = 18$ with the correct value of K_e results in underprediction of drag reduction, mean velocity and k^+ both in relation to the experimental data as well as in relation to the better prediction for $C = 45$.

The slope of the predicted *f–Re* curve in Fig. 2 is lower than that of the experiments although there is a small, but insufficient, improvement for $C = 45$. This value was chosen to match the *f–Re* predictions at a Reynolds number of around 42,900 with the experimental data; this is the flow condition for which there are experimental data on other flow properties. The differences in the mean velocity profile at a Reynolds number of 42,900 in Fig. 3 are consistent with the differences in the friction factor. For the turbulent kinetic energy profiles, plotted in Fig. 4, the changes are more dramatic. The turbulence model underpredicts both k/U^2 and k^+, with the effect of C being small in terms of the former and quite significant in terms of the latter. This is an indication that both models predict not too different values of k, but act strongly upon the friction velocity. In conclusion, by correcting the mistake of Cruz and Pinho [12] the true predictions of the flow of 0.125% PAA are of similar quality as those seen in that work for mean flow quantities, but are worse in terms of turbulent flow quantities.

Regarding the other fluids in Table 2, the corresponding predictions in Ref. [12] for $C = 18$ are correct but since the optimization of the turbulence model resulted in $C = 45$, the use of this value is to be preferred. As will be seen later in

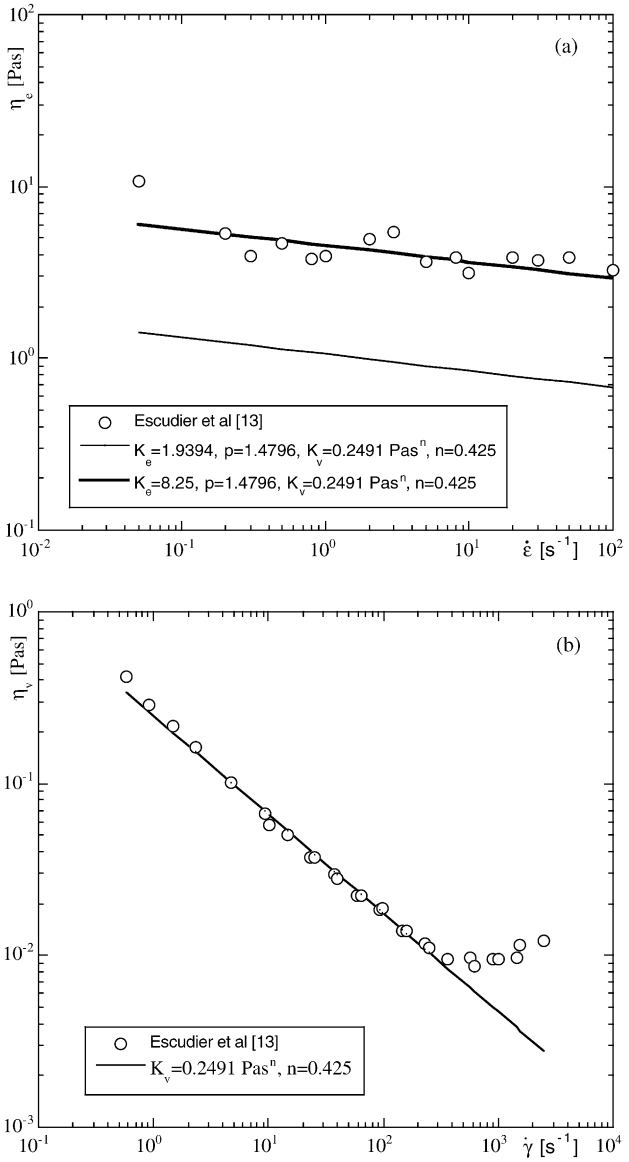

Fig. 1. Comparison between measured and fitted rheology for the 0.125% PAA solution: (a) extensional viscosity; (b) shear viscosity.

this paper, this is not just a formal issue; the use of $C = 45$ improves predictions for all the other fluids in the original turbulence model and is therefore beneficial for all the other fluids.

4.2. Effect of new stress

Fig. 2 includes predictions of friction factor by the new model for two different values of parameter C_0. Since at the outset the sign of the new stress is unknown, both possibilities had to be investigated. What is known is that under drag reducing conditions the Reynolds shear stress is strongly dampened and, because the viscous stress is low, there must be a compensating stress usually called polymer stress [17]. In the original turbulence model of Cruz and Pinho [12] it

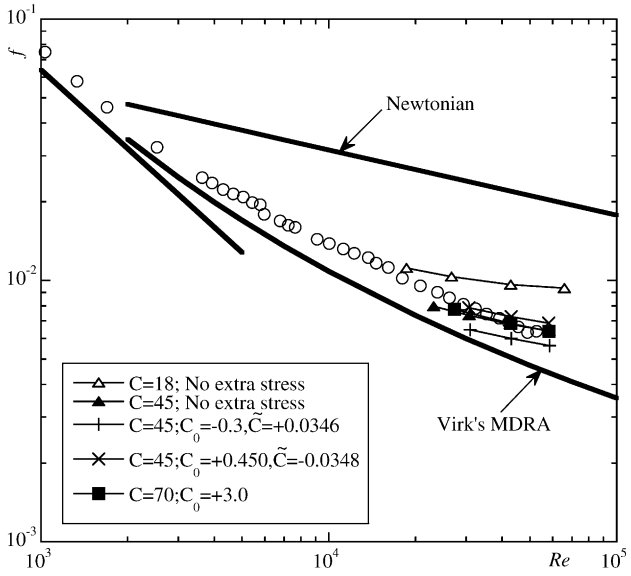

Fig. 2. Effect of C and of new stress on predictions of the friction factor for 0.125% PAA solution. Open circles are experimental data from Escudier et al. [13].

is the modified viscous stress that accounts for the difference between the total stress and the Reynolds shear stress. This may suggest that the new stress is positive, but this is not necessarily true: in a real drag reducing fluid the viscous stress is that due exclusively to the time-average shear flow, so the difference between the total and viscous stresses must be positive. Here, in contrast, it is not known how much of this polymer stress is being taken by the modified viscous stress ($2\bar{\mu}S_{ij}$) and so the new stress ($2\overline{\mu' s_{ij}}$) can in effect be negative, but its sum with the modified viscous stress must be a positive quantity.

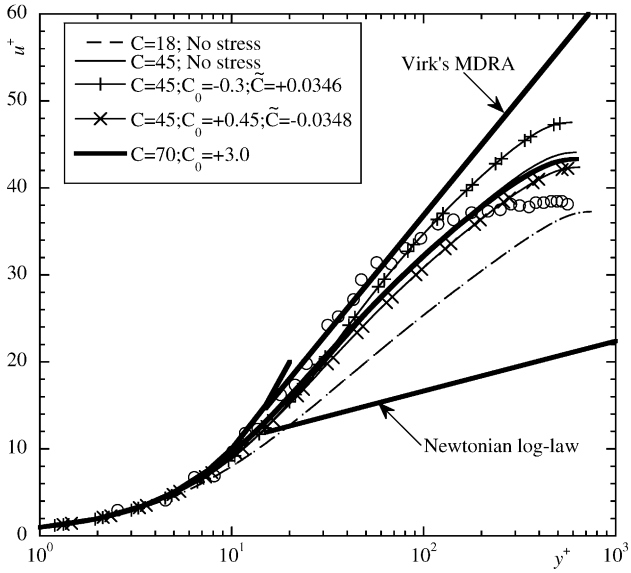

Fig. 3. Effect of C and of sign of new stress on predictions of the mean velocity profile for 0.125% PAA solution at $Re = 42{,}900$. Open circles are experimental data from Escudier et al. [13].

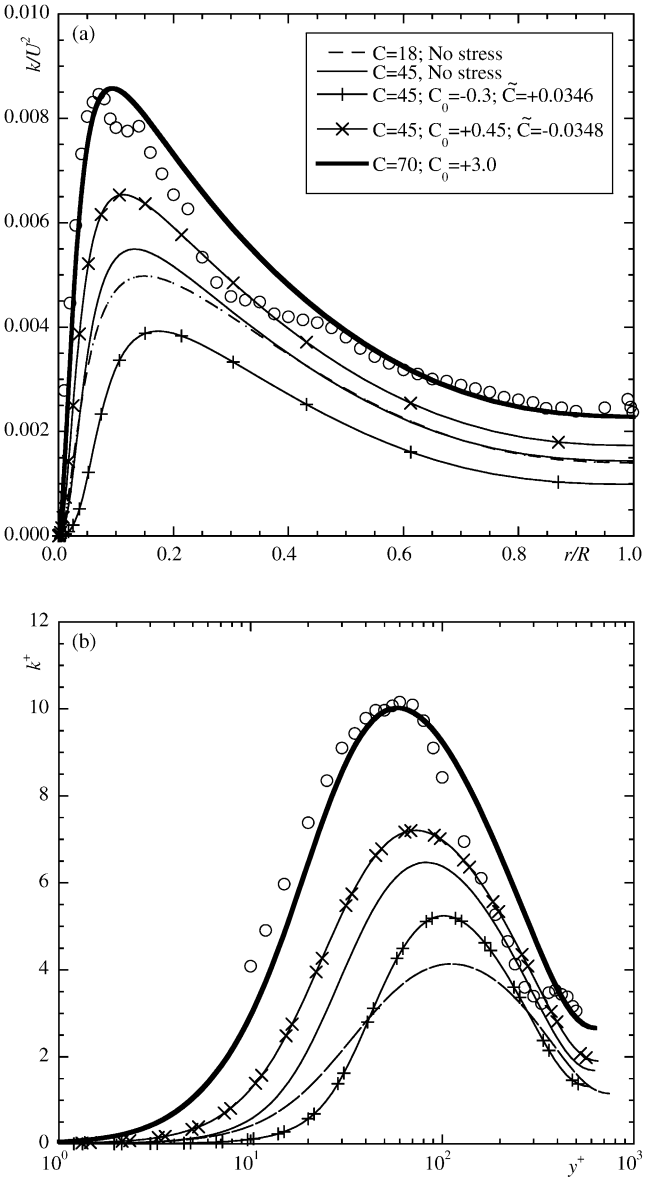

Fig. 4. Effect of C and of sign of new stress on predictions of the turbulent kinetic energy profiles for 0.125% PAA solution at $Re = 42{,}900$. Open circles are experimental data from Presti [14]: (a) physical normalisation; (b) wall normalisation.

The predictions with the new stress model in Figs. 2–4 show the effects of the sign and intensity of the new stress. The values of C_0 were such that the values of C are symmetric and the new stress has the sign of C. The positive new stress increases drag reduction, whereas a negative stress increases the fiction factor, with the former effect larger than the latter.

The corresponding predictions of the mean velocity profile in wall coordinates are plotted in Fig. 3. These are consistent with the predictions of the friction factor, with a higher shift of the profile towards Virk's asymptote for the positive stress (higher drag reduction) and a lower shift when the stress is negative. Again, the effect of the positive stress is larger than that of the negative stress.

For the turbulent kinetic energy, however, changes are dramatic. For the same cases, Fig. 4(a) and (b) compares simulations and experimental data and here the positive new stresses reduce the values of k, whereas negative stresses increase k. One of the shortcomings of the original model of Cruz and Pinho [12], here intensified by the increase of C to 45 discussed previously, is its underprediction of the turbulent kinetic energy. Now, a significant increase in k is obtained when the new stress is negative at the cost of deteriorating the predictions of f and u^+, but this can be easily corrected: as shown by Cruz and Pinho [12], an increase in the value of C reduces the friction factor while increasing k^+. Thus, combining a negative new stress with a higher value of C should improve predictions of k/U^2, and especially of k^+, while maintaining the performance of the model in terms of friction factor and mean velocity.

Before proceeding to suggest an adequate set of values for C and C_0, it is advantageous at to analyse in detail the radial profiles of the various shear stresses and these are shown in Fig. 5. It is clear from Fig. 5 that in spite of the very low value of the new stress, the Reynolds shear stress and the time-average viscous stress are strongly affected. Together with the zoom of Fig. 5(b) and (c), Fig. 5(a) shows the new stress to be non-zero, but small across the pipe, peaking only very close to the wall. Still, the impact of the new stress is dramatic. Inspection of the transport equation of k (Eq. (10)) helps understand this: the Reynolds shear stress acts to produce k, the viscous stress dissipates it and the new stress will dissipate energy if positive, but will create k if negative. The other contributions to the balance of k are less important. Very close to the wall, the magnitude of the new stress is similar to that of the Reynolds shear stress, regardless of its sign, so that when the new stress is positive it annihilates the effect of $-\rho\overline{uv}$ and production of turbulence is delayed until much farther away from the wall, thus leading to lower turbulence. Elsewhere, there is also a decrease in turbulence production since the new stress is non-zero, although small in magnitude. In contrast, when the new stress is negative production of k can increase significantly close to the wall and is increased elsewhere, raising the overall turbulence across the pipe.

Increasing C to 70 and considering a negative new stress with $C_0 = +3.0$, there is a significant improvement in the prediction of k/U^2 and k^+ while the quality of the remaining predictions (fRe and $u^+ - y^+$) is maintained. The friction factor in Fig. 2 matches the experiments at a Reynolds number in the vicinity of 42,000 as for the old model with $C = 45$. There is also good agreement for the mean velocity in Fig. 3, but the main benefit is in predicting the turbulent kinetic energy. As shown by the thick solid lines in Fig. 4(a) and (b), the predictions and the experimental data for k/U^2 and k^+ match well and it is especially noteworthy that not only the peak values, but also their locations, are well predicted.

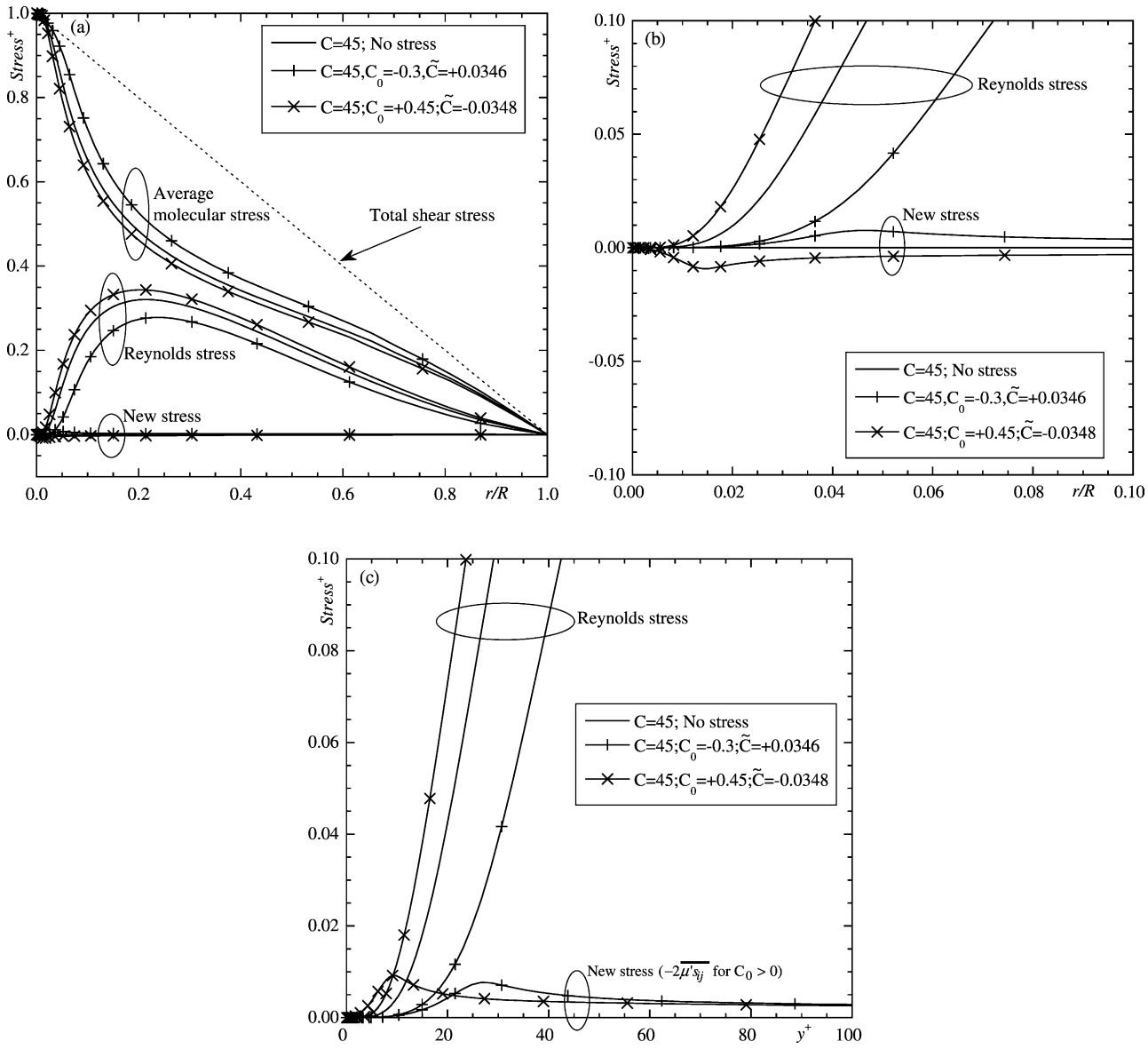

Fig. 5. Effect of C and of sign of new stress on the radial distribution of the various shear stresses across the pipe for flow of 0.125% PAA at $Re = 42{,}900$: (a) radial profile; (b) zoom in the near-wall region; (c) profile in wall coordinates (for $C_0 > 0$ $-2\overline{\mu' s_{ij}}$ is plotted).

These shear stress profiles may seem in contradiction with experimental [18,19] and DNS findings [20] of a strong Reynolds shear stress deficit and a large, so-called, polymer stress by comparison, especially close to maximum drag reduction conditions. However, this is not the case, as explained next. First, for none of the fluids and flow conditions here there are Reynolds shear stress data to make the adequate and meaningfull comparison. Secondly, Fig. 5(a) shows a dramatic decrease in the Reynolds shear stress relative to the total shear stress represented by the dashed line. As seen by Cruz and Pinho [12] (c.f. their Fig. 20), and in agreement with experimental data, at exactly the same high Reynolds number the Reynolds shear stress for a Newtonian fluid follows the total stress over 80% of the pipe (between the axis $r/R = 1$ and $r/R \approx 0.2$). Last, but not least, this Reynolds stress deficit is compensated by the sum $2\bar{\mu} S_{ij} + 2\overline{\mu' s_{ij}}$. These two stresses account for three effects which are combined in a complex manner: the viscous effect of the solvent, the viscous effect of the polymer and the elastic effect of the polymer, here due the strain-hardening of the Trouton ratio. Therefore, to compare meaningfully with the so-called polymer stress of the above-mentioned literature the difference between the total fluid shear stress and a pure viscous stress, either of the solvent or of the fluid, must be calculated, i.e., Eq. (35) in the former or Eq. (36) in the latter cases, respectively:

$$\tau_{ij,p} = 2\bar{\mu} S_{ij} + 2\overline{\mu' s_{ij}} - 2\mu_s S_{ij}, \tag{35}$$

$$\tau_{ij,p} = 2\bar{\mu} S_{ij} + 2\overline{\mu' s_{ij}} - 2\mu_v(S_{ij}) S_{ij}, \tag{36}$$

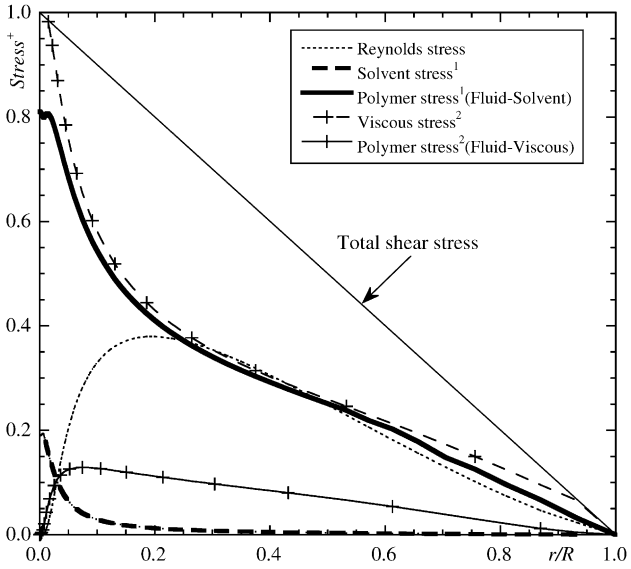

Fig. 6. Shear stress decomposition for 0.125% PAA at $Re = 42{,}900$ with $C = 70$ and $C_0 = +3$: case 1: according to Eq. (35); case 2: according to Eq. (36).

where μ_s is the solvent viscosity and $\mu_v(S_{ij})$ is the shear viscosity of the fluid calculated at the average value of the shear rate.

Fig. 6 compares the Reynolds shear stress with the polymer shear stress and the viscous shear stress calculated in both ways (Eqs. (35) and (36)) for the 0.125% PAA flow using the proposed turbulence model ($C = 70$ and $C_0 = +3$). The correct comparison with DNS simulations ([20] for instance) is using Eq. (35), represented as thick lines, and we clearly see the strong enhancement of the so-called polymer stress, which is as large as the Reynolds stress in this simulation. In an attempt to separate elastic effects from all the viscous effects Eq. (36) was also used to calculate another kind of polymer stress and the results are now represented by the thin lines. Now, the polymer stress is only about a third of the Reynolds stress, but this is still much larger than the new stress $2\overline{\mu' s_{ij}}$ as we can assess by comparing also with Fig. 5.

4.3. Performance of the model for the other fluids

In general, these improvements are consistent in that they take place with all fluids for which we possess experimental information. In Figs. 7–9, the performance of the new model is assessed by comparing its predictions with those of the previous turbulence model for $C = 18$ and $C = 45$ and with the experimental results of Escudier et al. [13] and Presti [14] for 0.25% CMC, a blend of 0.09%/0.09% XG/CMC and 0.2% XG, respectively. The corresponding rheological parameters are those listed in Table 2.

In all cases, there are improvements relative to the original model in Cruz and Pinho [12] ($C = 18$), both with the improved version of the original model ($C = 45$; $C_0 = 0$) as well as by the new model containing the new stress ($C = 70$; $C_0 = +3$). For the modified original model ($C = 45$), these improvements, assessed relative to the experimental data, mean a decrease in the friction factor, a larger upward shift of the mean velocity and a slight increase in turbulent kinetic energy. For the new model, however, sometimes there is a small deterioration in the prediction of f and u^+, but these are largely compensated by a significant improvement in predicting the turbulent kinetic energy.

For the 0.25% CMC solution, the friction factor in Fig. 7(a) increases slightly for the new stress model, and the mean velocity profile is correspondingly downshifted (c.f. Fig. 7(b)). These variations are very small in comparison to the increase in the turbulent quantities (k^+ and k/U^2) shown in Fig. 7(c) and (d). Both peak values of k are well predicted, but are farther from the wall than the experimental data.

For the blend of CMC and xanthan gum, the results in Fig. 8 show similar trends, but with less advantage coming from the new stress term. Here, the predictions of fRe and $u^+ - y^+$ for the new model are worse than those of the original model without the new stress ($C = 18$ and $C = 45$), although the difference is small. However, for the turbulent kinetic energy there is again a clear advantage in using the formulation with the new stress term. The peak in k/U^2 is now overpredicted by an amount similar to the underprediction of the peak by the two models with $C_0 = 0$, although all models overpredict the quantity elsewhere, but for k^+ there are important and larger improvements in terms of peak value, its location and the behaviour at low y^+. Considering the various positive and negative variations, the overall change was an improvement.

Finally, for the 0.2% XG in Fig. 9 net improvements are also observed. As with the previous two fluids, the use of the new stress slightly increases fRe relative to the corrected version of the original model of Cruz and Pinho [12] ($C = 45$; $C_0 = 0$) and this will correspond to a similar variation in the mean velocity profile (not shown). These variations are offset by dramatic changes in turbulent kinetic energy, whereas k/U^2 increases too much and is now in excess all across the pipe, the profile of k^+ has approached the measured data everywhere. The underprediction of k^+ is now basically a consequence of the underprediction of drag reduction as was also the case for the blend. As with the blend there is an overprediction of k/U^2 that must be taken care of in future developments.

5. Comparison with results of DNS simulations

An obvious question is how the predictions of this turbulence model compare with results from DNS simulations. The recent DNS simulations for viscoelastic fluids in the literature (see Section 1) assume that the fluids obey the FENE-P constitutive equation, but these were not fitted to experimental rheological data, in contrast to our turbulence model which was developed for a different kind of fluid

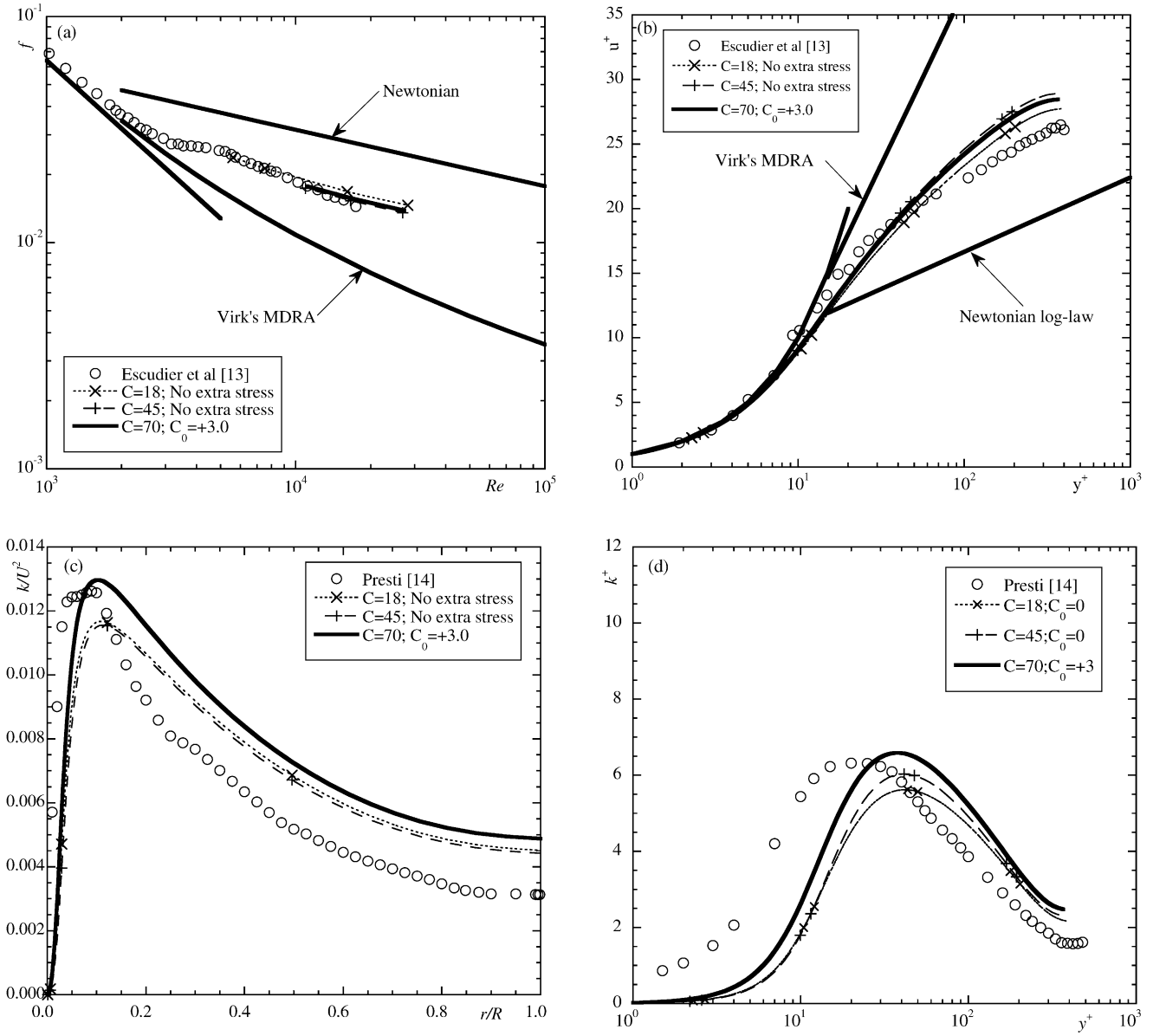

Fig. 7. Predictions of flow of 0.25% CMC at $Re = 16{,}600$ with the model with new stress ($C = 70$ and $C_0 = +3.0$) and comparisons with model of Cruz and Pinho [12] (old: $C = 18$ and $C_0 = +0.0$; corrected: $C = 45$ and $C_0 = +0.0$) and experimental data: (a) friction factor; (b) mean velocity profile; (c) turbulent kinetic energy in physical coordinates; (d) turbulent kinetic energy in wall coordinates.

and was calibrated assuming that the extensional viscosity in Escudier et al. [13] was properly measured. Nevertheless, it is important to make such an assessment to guide future research on turbulence modeling, regardless of its starting point being either the present work or a completely new kind of model based on the FENE-P constitutive equation. In any case, as we shall see, a major step forward must be our capability to correctly measure the extensional viscosity.

The channel flow test case of Dimitropoulos et al. [2] for the FENE-P model with $L = 10$, corresponding to mild drag reduction, was selected. The solvent and polymer viscosities were such that $\beta = 0.9$, the Weissenberg and Reynolds numbers based on the friction velocity and zero-shear viscosity were 50 and 125, respectively, and the Reynolds number based on the bulk velocity and channel half-height was equal to 1994 to which corresponded a drag reduction of 15% relative to Dean's correlation for the Darcy friction factor, Eq. (37). Our simulations were carried out in a channel of half-height (H) equal to 50.2 mm, an assumed fluid density of 1000 kg/m^3 and a total zero shear viscosity of 0.01 Pa s, so that the remaining characteristics were: $\eta_{p0} = 0.001$ Pas, $\eta_s = 0.009$ Pas, $\lambda = 0.806$ s and $U = 0.397$ m/s.

$$f_{\text{Dean}} = 0.292\, Re^{-1/4}. \tag{37}$$

The shear and extensional viscosities of the FENE-P model and the fitted power law expressions are plotted in Fig. 10(a)

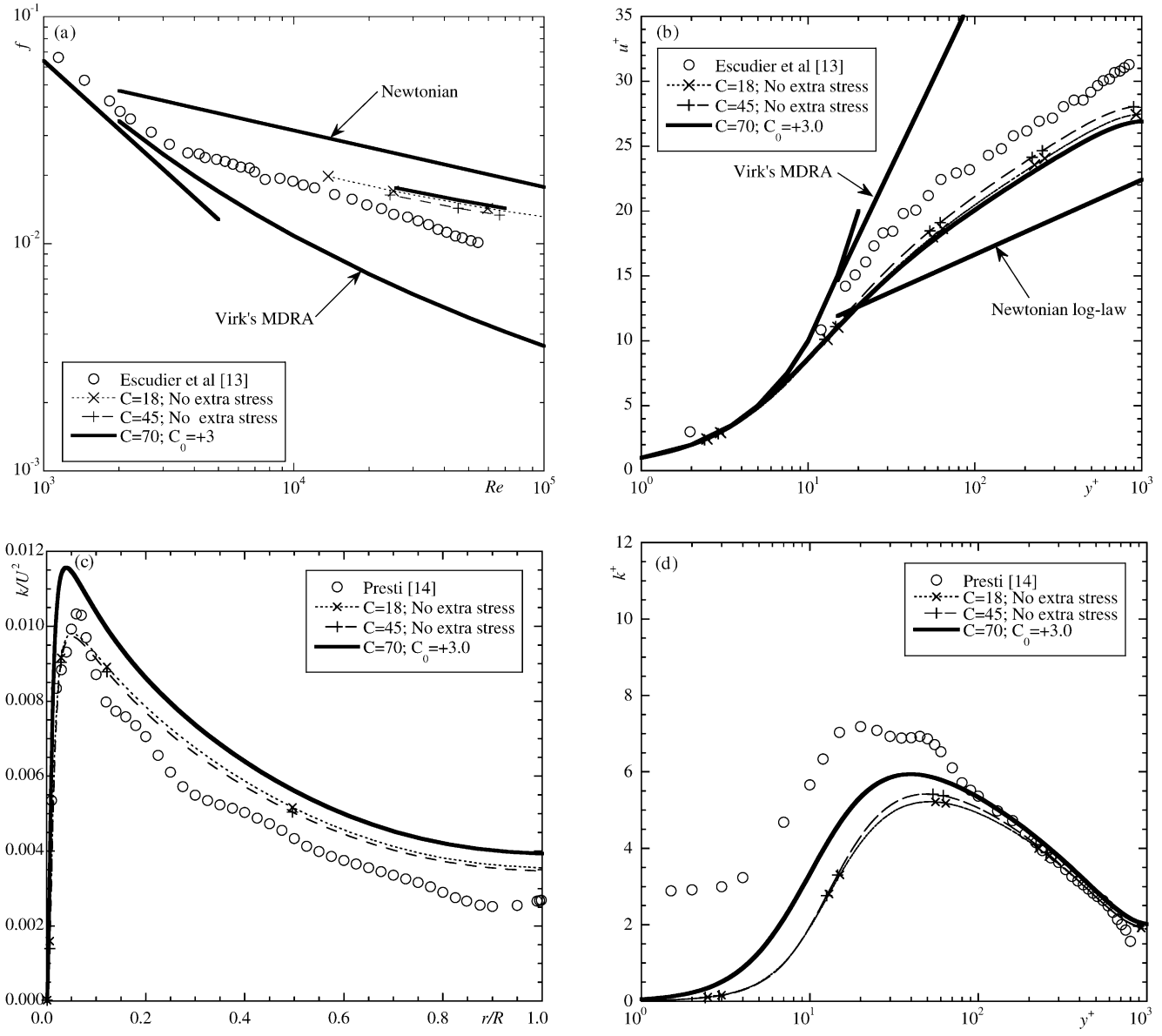

Fig. 8. Predictions of flow of 0.09%/0.09% CMC/XG at $Re = 45{,}300$ with the model with new stress ($C = 70$ and $C_0 = +3.0$) and comparisons with model of Cruz and Pinho [12] (old: $C = 18$ and $C_0 = +0.0$; corrected: $C = 45$ and $C_0 = +0.0$) and experimental data: (a) friction factor; (b) mean velocity profile; (c) turbulent kinetic energy in physical coordinates; (d) turbulent kinetic energy in wall coordinates.

and (b), respectively, and they show the first problem; whereas the shear viscosity is well represented by a power law, the extensional behaviour of the FENE-P model cannot be well fitted by a power law. This has to be contrasted with the good fittings with the experimental data in Fig. 1. The numerical simulation, for the same bulk velocity, resulted in the predictions in Table 3. Note that the Reynolds number, based on the wall viscosity, is not identical to that of the DNS simulations, based on the zero shear viscosity, but the difference is small and is of no consequence for the remaining comparisons and discussion.

The predicted drag reduction is more than twice that calculated by DNS (≈15%) and this is for the case where the extensional viscosity is fitted as in Fig. 10(b). Note also that the new model leads to a higher drag reduction than the original model of Cruz and Pinho for $C = 45$. The corresponding mean velocity and turbulent kinetic energy profiles are plotted in Fig. 11. The mean velocity data are consistent with the friction factor data in that to a higher drag reduction corresponds a higher upwards shift in the mean velocity

Table 3
Some bulk results of the simulation of the DNS case of Dimitropoulos et al. [2] for FENE-P model with $L = 10$ (DR = 15%)

Turbulence model	$Re = UH/\nu_w$	f	DR (%)
$C = 45$, $C_0 = 0$	2112	0.02741	36.4
$C = 70$, $C_0 = +3.0$	2111	0.02507	41.8

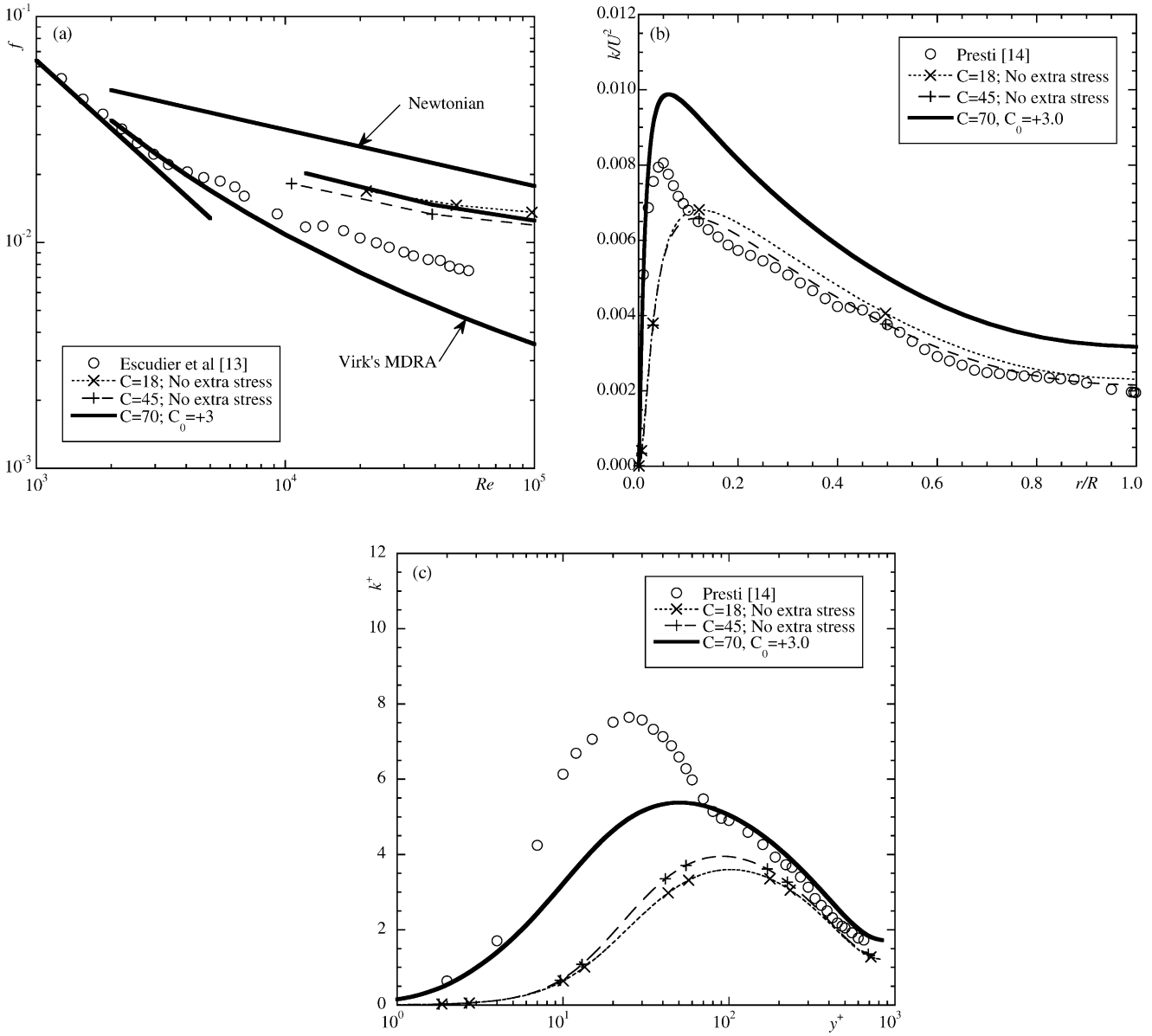

Fig. 9. Predictions of flow of 0.2% XG at $Re = 39{,}000$ with the new model ($C = 70$ and $C_0 = +3.0$) and comparison with model of Cruz and Pinho [12] (old: $C = 18$ and $C_0 = +0.0$; corrected: $C = 45$ and $C_0 = +0.0$) and experimental data: (a) friction factor; (b) turbulent kinetic energy in physical coordinates; (c) turbulent kinetic energy in wall coordinates.

profile. The turbulent kinetic energy is predicted reasonably well and suffers from some of the deficiencies seen above with the experimental fluids: the whole curve and the peak k^+ are shifted to higher y^+ and there is a small underprediction in the peak value of k^+. Since drag reduction is overpredicted, then the prediction of k is excessively dampened.

Numerical simulations were also attempted for other DNS cases, namely the FENE-P with $L = 30$ of Dimitropoulos et al. and the high drag reduction case of Ptasinski et al. [4] for $L = 31.7$; whereas for the $L = 30$ case a much higher drag reduction than given by DNS was predicted, as for $L = 10$, the Ptasinski et al. case always diverged because of excessive drag reduction by our model. So, for all cases there was a consistent pattern of excessive drag reduction prediction.

Had we fitted the extensional viscosity in a narrower range of shear/strain rates, to improve the fitting in the strain-hardening region, the exponent p would have been higher leading to even higher drag reductions. However, lower drag reductions, identical to those predicted by DNS, can be predicted if lower values of C are used but then the experimental cases of Escudier et al. [13] and Presti [14] would have been underpredicted. The present turbulence model, and that of Cruz and Pinho [12], were calibrated on the basis of the measurements of the extensional viscosity made by Escudier et al. [13] using opposed jet rheometry.

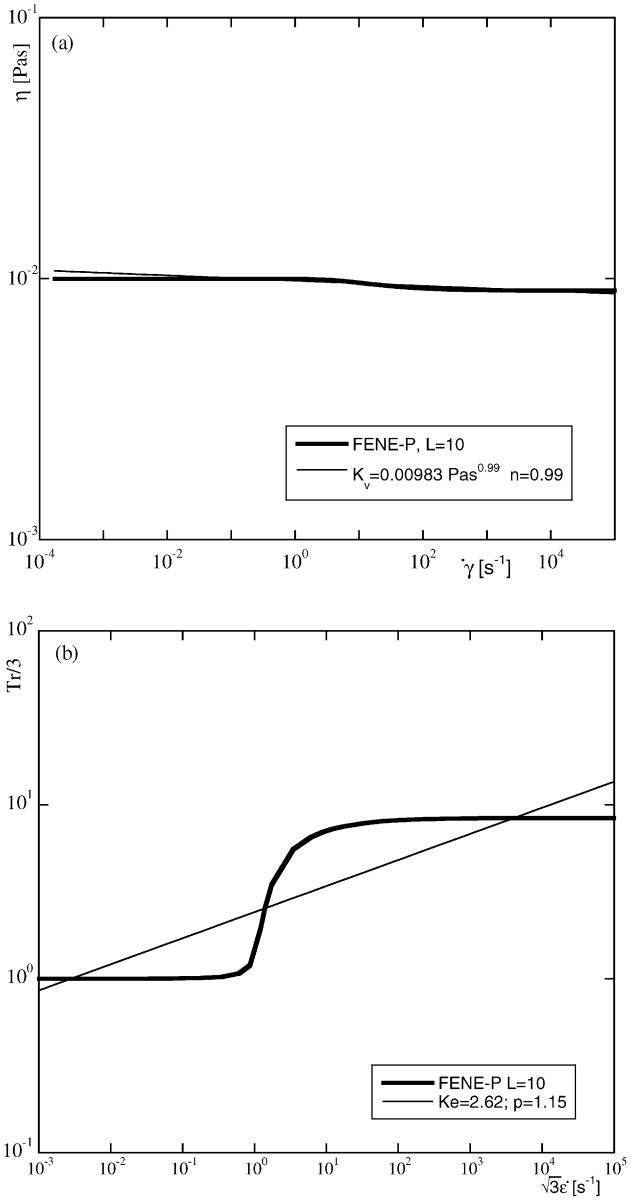

Fig. 10. Comparison between the steady viscosities for the FENE-P model of Dimitropoulos et al. [2] for $L = 10$ and the modified GNF model of Eq. (5): (a) shear viscosity; (b) extensional viscosity.

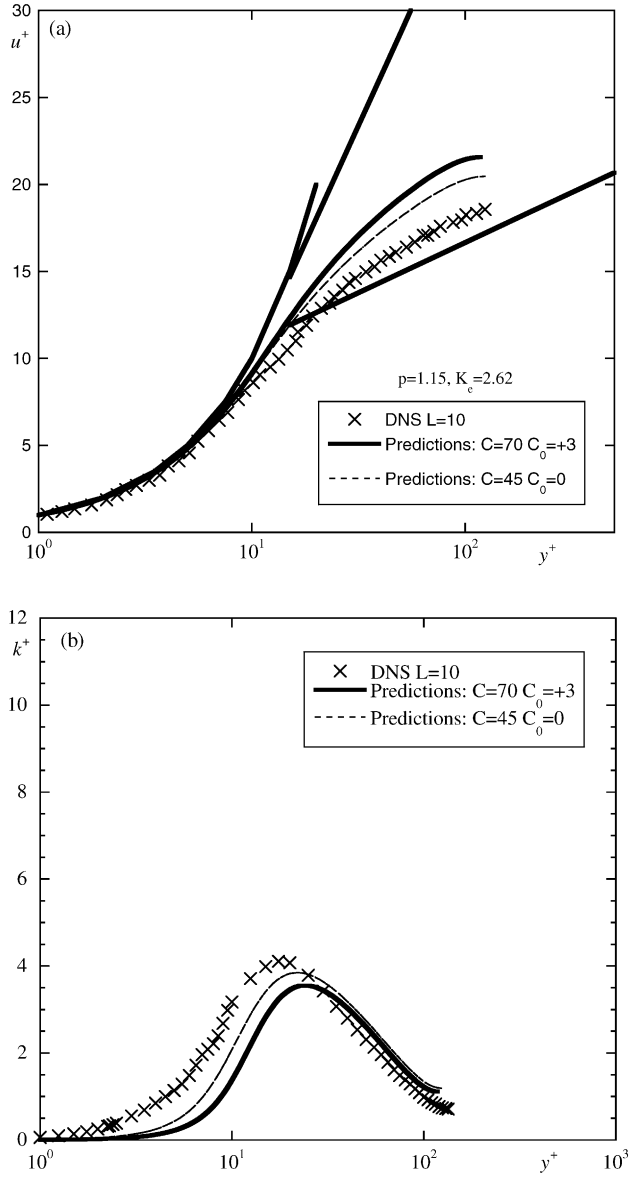

Fig. 11. Comparison between predictions and the results of the DNS simulations of Dimitropoulos et al. [2] for the FENE-P model with $L = 10$: (a) mean velocity profile in wall coordinates; (b) turbulent kinetic energy profile.

This technique is known to have deficiencies [21], but is still the best technique available to measure the extensional viscosity of dilute polymer solutions of low consistency over a wide range of strain rates. Simultaneously, the DNS studies are based on a constitutive model whose rheology has not been fully compared with that of real fluids, especially on what concerns extensional rheology, so statements of good performance of DNS based on comparison with experiments must also be critically assessed. Finally, the present turbulence model is also based on a constitutive equation that is not truly a viscoelastic model, but what is common to experiments, the DNS investigations and this family of turbulence models is an intense strain hardening of the extensional viscosity. Clearly, the development of turbulence models for drag reduction requires not only progress in turbulence modelling, but further progress is also essential in rheological modelling and in extensional rheology.

6. Conclusions

A turbulence model for drag reducing viscolastic fluids was improved by inclusion, in the momentum and turbulent kinetic energy equations, of the new stress term previously neglected by Cruz and Pinho [12]. The new stress accounts for the correlation between fluctuations of viscosity

and fluctuations of the rate of deformation and a model was developed here for the new stress in order to close the full set of equations. However, prior to testing this new turbulence model, the original value of K_e for 0.125% PAA used by Cruz and Pinho was corrected and this lead to an increase in C to 45 for improved predictions.

Calibration of the new turbulence model against experimental data for a solution of 0.125% PAA gave $C = 70$ in the damping function f_μ and $C_0 = +3.0$ for the new stress closure. The model was then tested by comparison with experimental data from other fluids.

The advantage of this new model over that of Cruz and Pinho is the improvement in the distribution of turbulent kinetic energy, and especially of k^+, while decreasing only slightly the quality of the predictions for the other quantities (f and u^+). However, in some cases k/U^2 was overpredicted and this requires future modifications. These improvements were found to be general, happening with all fluids tested. The decomposition of the total shear stress into a Reynolds stress, a solvent viscous stress and a polymer stress has shown the strong Reynolds stress deficit accompanied by a large polymer stress that is much higher than the new stress. This polymer stress is of the same magnitude as the Reynolds stress in the core of the pipe but is much higher near the wall, and these observations agree with results from DNS simulations. Finally, predictions were carried out for a case from the literature where DNS has been performed and the turbulence model showed excessive drag reduction. This was possibly a consequence of the different quality of extensional viscosity data available in experiments and inherent to the FENE-P model.

It is clear at this stage that further modifications of the current turbulence model are required in order to bring predictions into agreement with experiments for all fluids. This may require modifications to some parameters of the model, making them dependent of the fluid rheology, or the introduction of less fluid-dependent changes, such as the use of terms to deal with anisotropic behaviour. The comparison with DNS results has also underlined the need for improvements in extensional rheometry, constitutive modelling and turbulence modeling.

Acknowledgements

The authors wish to thank CNPq of Brasil and ICCTI of Portugal for funding the exchange programme Project 2001 Proc C 4.3.1. F.T. Pinho and P.R. Resende also acknowledge the funding of FEDER and Fundação para a Ciência e Tecnologia through grants POCTI 37699/EQU/2001 and POCTI 37711/EME/2001 and of CRUP via Action B-5/03 of exchange with the UK for discussions with Prof. M.P. Escudier (University of Liverpool, UK). We are also in debt to Prof. B.A. Younis (U. California Davis, USA) for making available a code for the simulations.

References

[1] F.T. Pinho, A GNF framework for turbulent flow models of drag reducing fluids and proposal for a k-ε type closure, J. Non-Newt. Fluid Mech. 114 (2003) 149–184.
[2] C.D. Dimitropoulos, R. Sureshkumar, A.N. Beris, Direct numerical simulation of viscoelastic turbulent channel flow exhibiting drag reduction: effect of the variation of rheological parameters, J. Non-Newt. Fluid Mech. 79 (1998) 433–468.
[3] E. De Angelis, C.M. Casciola, R. Piva, DNS of wall turbulence: dilute polymers and self-sustaining mechanisms, Comput. Fluids 31 (2002) 495–507.
[4] P.K. Ptasinski, B.J. Boersma, F.T.M. Nieuwstadt, M.A. Hulsen, B.H.A.A. Van Den Brule, J.C.R. Hunt, Turbulent channel flow near maximum drag reduction: simulation, experiments and mechanisms, J. Fluid Mech. 490 (2003) 251–291.
[5] Q. Zhou, R. Akhavan, A comparison of FENE and FENE-P dumbbell and chain models in turbulent flow, J. Non-Newt. Fluid Mech. 109 (2003) 115–155.
[6] G. Lielens, R. Keunings, V. Legat, The FENE-L and FENE-LS closure approximations to the kinetic theory of finitely extensible dumbbells, J. Non-Newt. Fluid Mech. 87 (1999) 179–196.
[7] P.A. Stone, M.D. Graham, Polymer dynamics in a model of the turbulent buffer layer, Phys. Fluids 15 (5) (2003) 1247–1256.
[8] J.M.J. Den Toonder, F.T.M. Nieuwstadt, G.D.C. Kuiken, The role of elongational viscosity in the mechanism of drag reduction by polymer additives, Appl. Sci. Res. 54 (1995) 95–123.
[9] J.M.J. Den Toonder, M.A. Hulsen, G.D.C. Kuiken, F.T.M. Nieuwstadt, Drag reduction by polymer additives in a turbulent pipe flow: numerical and laboratory experiments, J. Fluid Mech. 337 (1997) 193–231.
[10] R. Sureshkumar, A.N. Beris, R.A. Handler, Direct numerical simulation of the turbulent channel flow of a polymer solution, Phys. Fluids 9 (1997) 743–755.
[11] J.L. Lumley, Drag reduction by additives, Ann. Rev. Fluid Mech. 1 (1969) 367–386.
[12] D.O.A. Cruz, F.T. Pinho, Turbulent pipe flow predictions with a low Reynolds number k-ε model for drag reducing fluids, J. Non-Newt. Fluid Mech. 114 (2003) 109–148.
[13] M.P. Escudier, F. Presti, S. Smith, Drag reduction in the turbulent pipe flow of polymers, J. Non-Newt Fluid Mech. 81 (1999) 197–213.
[14] F. Presti, Investigation of transitional and turbulent pipe flow of non-Newtonian fluids, Ph.D. Thesis, University of Liverpool, UK, 2000.
[15] Y. Nagano, M. Hishida, Improved form of the k-ε model for wall turbulent shear flows, J. Fluids Eng. 109 (1987) 156.
[16] H. Tennekes, J.L. Lumley, A First Course in Turbulence, MIT Press, 1972.
[17] B.A. Younis, A computer programme for two-dimensional turbulent boundary layer flow, Internal Report, Department of Civil Engineering, City University, London, UK, 1987.
[18] M.D. Warholic, H. Massah, T.J. Hanratty, Influence of drag reducing polymers on turbulence: effects of Reynolds number, concentration and mixing, Exp. Fluids 27 (1999) 461–472.
[19] M. Vlachogiannis, T.J. Hanratty, Influence of wavy structured surfaces and large scale polymer structures on drag reduction, Exp. Fluids 36 (2004) 685–700.
[20] P.K. Ptasinski, F.T.M. Nieuwstadt, B.H.A.A. Van Den Brule, M.A. Hulsen, Experiments in turbulent pipe flow with polymer additives at maximum drag reduction, Flow Turbul. Combust. 66 (2001) 159–182.
[21] P. Dontula, M. Pasquali, L.E. Scriven, C.W. Macosko, Can extensional viscosity be measured with opposed-nozzle devices? Rheol. Acta 36 (1997) 429–448.